Null Point Imaging: A Joint Acquisition/Analysis Paradigm for MR Classification

Alain Pitiot[1], John Totman[1], and Penny Gowland[2]

[1] Brain & Body Centre
[2] Sir Peter Mansfield Magnetique Resonance Centre
University of Nottingham, UK
{alain.pitiot,john.totman,penny.gowland}@nottingham.ac.uk

Abstract. Automatic classification of neurological tissues is a first step to many structural analysis pipelines. Most computational approaches are designed to extract the best possible classification results out of MR data acquired with standard clinical protocols. We observe that the characteristics of the latter owe more to the historical circumstances under which they were developed and the visual appreciation of the radiographer who acquires the images than to the optimality with which they can be classified with an automatic algorithm.

We submit that better performances could be obtained by considering the acquisition and analysis processes *conjointly* rather than optimising them independently. Here, we propose such a joint approach to MR tissue classification in the form of a fast MR sequence, which nulls the magnitude and changes the sign of the phase at the boundary between tissue types. A simple phase-based thresholding algorithm then suffices to segment the tissues. Preliminary results show promises to simplify and shorten the overall classification process.

1 Introduction

The explosive growth in medical imaging technologies such as Magnetic Resonance Imaging MRI), computer assisted tomography (CT) or positron emission tomography (PET) has fuelled an unprecedented drive to explore the structural and functional organization of the human body. Arguably one of the most complex organs, the human brain has been the primary beneficiary of these fast paced developments. A major objective of neuroscience is to understand both the anatomical characteristics of the various structures of the brain and their inter-relationships. From the structural standpoint (our main focus here), this ambitious goal is often translated into statistical analysis of anatomical variability, within groups, through development, or between normal and diseased populations [1]. A pivotal first step to most MR based structural studies, automatic tissue classification forms the basis for a variety of neuro-informatics applications: quantitative measurement of tissue loss or gain in healthy and diseases populations [2], analysis of cortical thickness and folding [3], automated diagnosis of diseases [4], or morphological analysis such as voxel based morphometry [5] amongst others.

N. Ayache, S. Ourselin, A. Maeder (Eds.): MICCAI 2007, Part I, LNCS 4791, pp. 759–766, 2007.

Formally, tissue classification consists in partitioning the input brain MR volume into disjoint regions corresponding to the three main tissue types: white matter (WM), gray matter (GM) and cerebro-spinal fluid (CSF). Non brain tissues such as bone, skin, dura or the meninges are often collected into a fourth category ("other").

A whole menagerie of image analysis techniques are available to classify brain tissues from either monospectral (often T1-weighted MRI) or multisprectral MR images. They rely on a no less varied selection of parametric and non-parametric statistical classifiers, from k-nearest neighbours [6] to neural networks [7]. The necessity to deal with intensity inhomogeneities (bias field) and partial volume effect voxels (those voxels that contain a mixture of several tissue types) called for techniques capable of estimating the relative fraction of each tissue class in each voxel. EM-type algorithms and Hidden Markov Random Field approaches [8,9,10] in particular have proved very popular (see [11] for a thorough review of classification approaches).

1.1 Sub-optimality of Independent Acquisition and Analysis

For a variety of logistics and historical reasons, developments in computational tissue classification have been mostly limited to the processing of clinical MR sequences (i.e. sequences developed specifically for clinical applications) independently of their optimality in distinguishing between tissue types.

As an illustration, the now standard T1/T2/PD multispectral acquisition protocol comes from an era when most brain sequences were based on Spin Echo imaging. Though time consuming, Spin Echo produced good tissue contrast and allowed for the simultaneous acquisition of T2-weighted and proton density (PD) images. The latter provided useful additional information for pathologies. With the development of faster Turbo/Fast Spin Echo sequences, this speed-up trick was not available any longer. However PD had already become part of the standard protocol, causing an effective doubling of the (admittedly now shorter) examination time. Meanwhile, most modern T1 sequences now rely on the even faster 3D Gradient Echo imaging, which also allows for much higher resolution than 2D slice based approaches like Fast Spin Echo.

Incidentally, while the T1/T2/PD combination of contrasts often yields good classification results, other spectral combinations offer markedly better classification performances over acquisition time ratios. For example, the joint use of standard anatomical protocols and contrast-enhanced sequences has proved particularly efficient in cancer and multiple sclerosis research [12].

Regrettably, we note that all too often, analysis only follows acquisition, in that the parameters of the MR sequences are optimized *before* the analysis, following criteria best suited for human operators, not algorithms. For instance, a radiographer or physicist in charge of an MR scanner will often strive to achieve the best visual compromise between contrast and noise whereas, from a computational standpoint, within-class noise matters less than interclass separability.

1.2 A Joint Approach to Classification

We submit that better overall results could be obtained by considering the acquisition and analysis processes *conjointly* rather than optimising them independently. Here we propose such an approach developed specifically for tissue classification in cerebral MR imaging. It consists of a novel MR sequence, which we dubbed Null Point Imaging (NPI), and a very simple phase-based classification algorithm. By imaging half way between the GM and WM null points (see below for detail), the proposed MR sequence introduces *at the acquisition stage* a nulled boundary layer between GM and WM tissues. This layer coincides with the partial volume effects (PVE) voxels resulting from the mix of GM and WM along the gray/white surface. Remarkably, because we image between the two null points, the phase image acquired with this protocol is positive for predominantly gray voxels and negative for predominantly white voxels, which makes it trivial to segment once unwrapped. Using the same principle we also introduce a boundary layer between GM and CSF and segment them in phase space.

We first describe our joint acquisition/analysis approach in Section 2 before presenting the first classification results and some elements of validation in Section 3.

2 Method

2.1 Imaging Brain Tissues with MR

When placed in the strong magnetic field of the scanner (B_0), hydrogen nuclei (protons) align so as to create a net equilibrium magnetization (M_0), parallel to the applied magnetic field, the longitudinal direction. Excitation of the protons by a radio frequency pulse will tip this net magnetization away from the longitudinal direction, and the time taken for the magnetization to recover to its equilibrium value M_0 is characterized by the longitudinal recovery time T1 . In standard T1-weighted imaging, tissue contrast is created by the differences in T1 between different tissues. Figure 1(a) plots the recovery of the longitudinal magnetization for GM, WM and CSF as a function of time, after an RF pulse that had inverted the longitudinal magnetization at $t = 0s$.

In most clinical sequences, imaging is performed at the point in time where the difference between the longitudinal magnetization of WM, GM and CSF is greatest ($960ms$ in Figure 1(a)).

A common technique to increase contrast, inversion recovery uses a preparatory RF pulse to rotate the net magnetization 180^o down the B_0 axis. Before the magnetization reaches its equilibrium, another RF pulse is applied at time TI seconds. The preparatory pulse greatly lengthens the duration of the recovery process and consequently increases the contrast between tissues. Remarkably, while the direction of the net magnetization changes sign with this technique, its modulus seems to drop to a null point before recovering. This effect has been exploited in sequence development as a means to selectively remove signal from particular tissue types. In a classical MPRAGE sequence for instance (a fast high-resolution T1-weighted 3D sequence [13]) , TI is chosen to coincide with the time at which contrast is maximum after the initial inversion pulse ($960ms$).

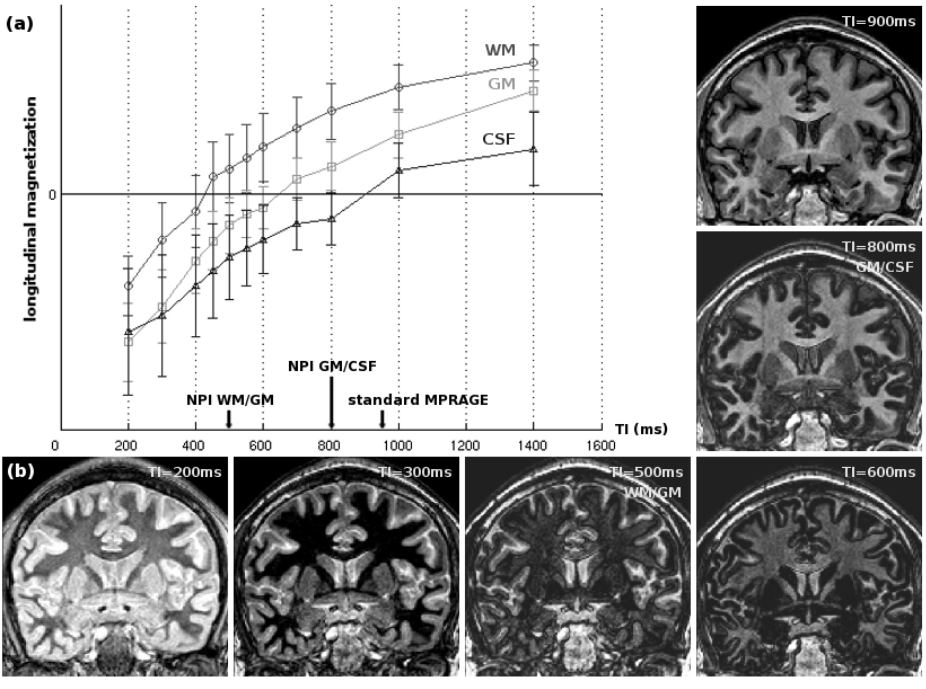

Fig. 1. Imaging characteristics of a standard MPRAGE sequence for various values of TI: (a) longitudinal magnetization (mean and standard deviation) of GM,WM and CSF as a function of the TI parameter; (b) sagittal sections of rigidly registered scans of the same volunteer's brain for different TIs

2.2 Imaging Tissue Boundaries with NPI

Here, we propose to use this nulling effect as a means to classify brain tissues. Our Null Point Imaging sequence is an MPRAGE sequence whose TI value is the barycentre of the GM and WM null points. Since the net magnetization vectors of GM and WM have the same modulus and different signs at that point, the MR signal of those partial volume effect voxels which contain a equal mixture of both GM and WM is nulled. This creates a black line between GM and WM voxels in the modulus image (see middle column of Figure 2). It also makes for a particularly "classification friendly" phase image where GM voxels have negative values and WM voxels positive ones, once the phase has been unwrapped [14]. We then segment the input volume by thresholding the unwrapped phase image at zero. Note that even though tissue contrast between GM and WM is almost null, this does not impact the performance of our classifier since thresholding is done in phase space. Alternatively, by selecting a TI value half way between the GM and CSF null points, our NPI technique outlines in black the pial surface (GM/CSF boundary) and a similar phase-based thresholding approach enables the segmentation of GM and CSF.

Determining the optimal TI value for the NPI sequence is a simple three-stepped approach. First, we acquire a series of structural images of a volunteer's brain by varying the TI parameter of a conventional T1-weighted sequence. All acquisitions were performed on a Philips Achieva, 1.5T with an 8-channel SENSE head coil. Note that we chose MPRAGE as our base sequence even though any inversion recovery sequence could have been employed. We then classify the volume corresponding to the standard clinical choice of TI (TI = $960ms$ for maximal contrast between WM,GM and CSF) using a standard off-the-shelf tissue classification technique (in our case, the MNI neural network classifier [7]). From these GM, WM and CSF maps, we compute the average intensity value per tissue for each value of TI (see Figure 1(a)). Finally, we determine the optimal value for TI by estimating the zero crossing point for the GM, WM and CSF curves and computing their barycentres. Note that although there is some inter- and intra- individual variation in T1 times for these tissue types it has been shown to be fairly uniform in the absence of pathology. Therefore, this optimization process only needs to be done once per scanner, on a limited number of brains.

From Figure 1(a), we get: $TI = 500ms$ for GM/WM segmentation and $TI = 800ms$ for GM/CSF segmentation. This can be visually confirmed on Figure 1(b) where a black line indeed separates GM from WM at $500ms$ and GM from CSF at $800ms$.

Note that as opposed to susceptibility weighted imaging [15] which uses naturally occurring phase variation to enhance the quality of the acquired magnitude images, our approach imposes a specific phase contrast.

3 Results

Figure 2 illustrates on a volunteer's brain the ability of our NPI approach to distinguish between WM, GM and CSF voxels. We show on the left column a selection of sagittal, coronal and axial slices cut through a standard T1-weighed volume, the corresponding section (after rigid registration) through the NPI magnitude at $TI = 500ms$ (black line between GM and WM) in the middle and the classification maps on the right column (CSF is black, GM is gray and WM is white). Note that we skull-stripped the classification maps in the interest of visual clarity.

3.1 Elements of Validation

Since our joint acquisition/analysis approach is based on a custom MR sequence, we did not have the possibility of using brain simulators (e.g. BrainWeb [16]) to estimate its performances. In the absence of a gold standard, we used as a straw-man standard the classification maps obtained with a standard classification package (the MNI neural network classifier [7]) on the average of 5 rigidly registered standard T1 + T2/PD scans of the same volunteer's brain. The increased signal to noise ratio of the average image yielded an adequate classification against which

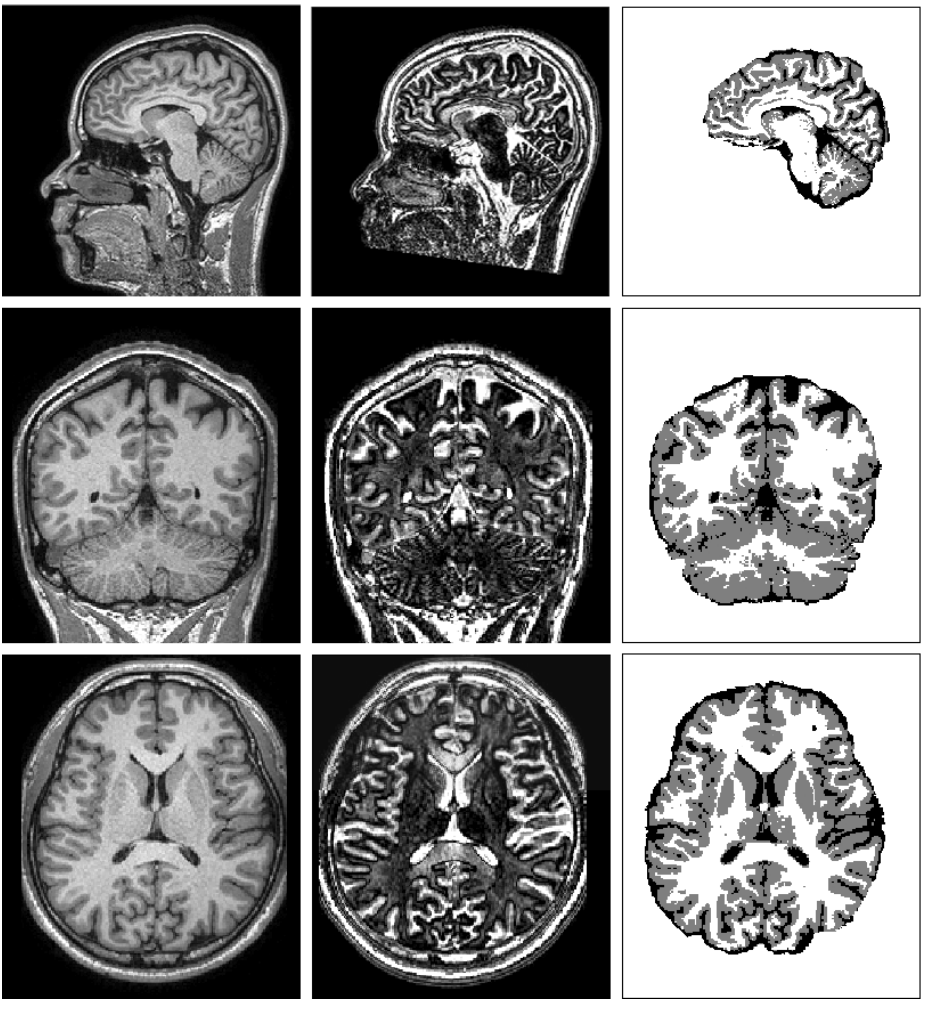

Fig. 2. A selection of corresponding slices cut through the same volunteer's brain: standard T1-weighted sequence (left column); NPI sequence with $TI = 500ms$, a black line follows the GM/WM boundary (center column); binary classification map (right column)

we compared the maps obtained with our approach on two NPI scans of the same volunteer (NPI with $TI = 500ms$ and with $TI = 800ms$).

Following Van Leemput et al. [9], we used the Dice metric [17]. Let Map_T^{mni} denote the classification map for tissue T obtained with the selected standard package, and let Map_T^{npi} be the NPI classification map. The Dice metric is given by: $D_T = 2|Map_T^{mni} \cap Map_T^{npi}|/(|Map_T^{mni}| + |Map_T^{npi}|)$ where $|.|$ is the set size operator.

Overall, our fast, phase-based thresholding approach gave, with only 2 images, results remarkably close to those obtained with the sophisticated MNI classifier

on the average images ($D_{WM} = 84\%$, $D_{GM} = 82\%$ and $D_{CSF} = 72\%$). Visual inspection confirmed this finding and showed that discrepancies where for the most part due to isolated voxels (these could be corrected with a morphological filter), overestimation of CSF in the temporal lobes (due to issues with phase unwrapping in the presence of scanner inhomogeneities), and differences in areas where the MNI approach was arguably wrong (in particular around some of the deep gray nuclei -thalamus- for GM).

4 Conclusion

We have presented a joint acquisition/analysis approach to MR tissue classification where information obtained in a preliminary analysis stage (graph of longitudinal magnetization as a function of TI parameter) helped optimize the acquisition sequence. In turn, the acquired images proved much easier to classify than standard T1-weighted or T2/PD multispectral sequences. Indeed, the phase image changed sign at the transition between predominantly gray and predominantly white PVE voxels, which yielded a very simple thresholding algorithm.

Our NPI classification technique is particularly efficient with respect to standard approaches. Typically, on a Philips 1.5T scanner, one or two $15mn$ long scans ($1mm^3$ isotropic T1-weighted sequence for monospectral and/or a $1 \times 1 \times 2mm$ T2/PD sequence for multispectral) followed by sophisticated image processing could be replaced by two fast $6mn$ sequences with a trivial classification algorithm. Note that in a standard computational pipeline, T1-weighted images are often used for other purposes than just classification: for instance they serve to extract the brain from the skull, or to correct for intensity inhomogeneities. Incidentally, even though our approach is not intended for use as a diagnostic tool, its behaviour in the presence of pathological defects such as lesions or tumours would be worth evaluating.

Preliminary results are very encouraging and show performances on par with a standard package even without any pre- or post-processing (inhomogeneity correction or morphological filtering for instance). We are currently working on a thorough validation where comparison against a variety of publicly available classifiers will be performed within the STAPLE framework [18].

Finally, we are also exploring the possibility of using the phase value in each voxel to roughly estimate the mixture of tissues within that voxel, rather than simply thresholding the phase image at zero to obtain a ternary classification map.

References

1. Toga, A., Mazziotta, J.: Brain Mapping: The Methods. Academic Press, London (2002)
2. Thompson, P., Hayashi, K., de Zubicaray, G., Janke, A., Rose, S., Semple, J., Hong, M., Herman, D., Gravano, D., Dittmer, S., Doddrell, D., Toga, A.: Dynamics of Gray Matter Loss in Alzheimer's Disease. Journal of Neuroscience 23, 994–1005 (2003)

3. Fischl, B., Dale, A.: Measuring the Thickness of the Human Cerebral Cortex from Magnetic Resonance Images. Proceedings of the National Academy of Sciences 97, 11044–11049 (2000)
4. Stoeckel, J., Malandain, G., Migneco, O., Koulibaly, P., Robert, P., Ayache, N., Darcourt, J.: Classification of SPECT Images of Normal Subjects versus Images of Alzheimer's Disease Patients. In: Niessen, W.J., Viergever, M.A. (eds.) MICCAI 2001. LNCS, vol. 2208, pp. 666–674. Springer, Heidelberg (2001)
5. Ashburner, J., Friston, K.: Voxel-based morphometry: the methods. NeuroImage 11, 805–821 (2000)
6. Warfield, S.K.: Fast k-NN classification for multichannel image data. Pattern Recognition Letters 17, 713–721 (1996)
7. Collins, D.L., Zijdenbos, A.P., Baaré, W.F.C., Evans, A.C.: ANIMAL+INSECT: Improved Cortical Structure Segmentation. In: Proc. of IPMI 1999, pp. 210–223 (1999)
8. Held, K., Kops, E., Krause, B., Wells, W., Kikinis, R., Müller-Gärtner, H.: Markov random field segmentation of brain MR images. IEEE Transactions on Medical Imaging 16 (1997)
9. Leemput, K.V., Maes, F., Suetens, P.: Automated model-based tissue classification of MR images of the brain. IEEE trans. on medical imaging 18, 897–908 (1999)
10. Zhang, Y., Brady, M., Smith, S.: Segmentation of brain MR images through a hidden markov random field model and the expectation-maximization algorithm. IEEE trans. on medical imaging 20, 45–57 (2001)
11. Pham, D., Xu, C., Prince, J.: Current Methods in Medical Image Segmentation. Annual Reviews 2, 315–337 (1996)
12. Dugas-Phocion, G., Lebrun, C., Chanalet, S., Chatel, M., Ayache, N., Malandain, G.: Automatic segmentation of white matter lesions in multi-sequence MRI of relapsing-remitting multiple sclerosis patients. In: ECTRIMS, Thessaloniki, Greece (2005)
13. Brant-Zawadzki, M., Gillan, G., Nitz, W.: MP RAGE: a three-dimensional, T1-weighted, gradient-echo sequence– initial experience in the brain. Radiology 182, 769–775 (1992)
14. Xu, W., Cumming, I.: A region growing algorithm for insar phase unwrapping. IEEE Trans. Geosci. Remote Sensing 37, 124–134 (1999)
15. Haacke, E., Xu, Y., Cheng, Y., Reichenbach, J.: Susceptibility weighted imaging (SWI). Magnetic Resonance Imaging 52, 612–618 (2004)
16. Collins, D., Zijdenbos, A., Kollokian, V., Sled, J., Kabani, N., Holmes, C., Evans, A.: Design and Construction of a Realistic Digital Brain Phantom. IEEE Transactions on Medical Imaging 26, 463–468 (1998)
17. Dice, L.: Measures of the amount of ecologic association between species. Ecology 26, 297–302 (1945)
18. Warfield, S.K., Zou, K.H., Wells, W.M.: Simultaneous truth and performance level estimation (STAPLE): an algorithm for the validation of image segmentation. IEEE Trans. Med. Imaging 23, 903–921 (2004)